

to appear in the *Astronomical Journal*

Ages of White Dwarf-Red Subdwarf Systems

Hektor Monteiro¹, Wei-Chun Jao¹, Todd Henry¹, John Subasavage¹, and Thom Beaulieu¹

Georgia State University, Atlanta, GA 30302-4106

ABSTRACT

We provide the first age estimates for two recently discovered white dwarf-red subdwarf systems, LHS 193AB and LHS 300AB. These unusual systems provide a new opportunity for linking the reliable age estimates for the white dwarfs to the (measurable) metallicities of the red subdwarfs. We have obtained precise photometry in the $V_JR_{KC}I_{KC}JH$ bands and spectroscopy covering from 6000Å to 9000Å for the two new systems, as well as for a comparison white dwarf-main sequence red dwarf system, GJ 283 AB. Using model grids available in the literature, we estimate the cooling age as well as temperature, surface gravity, mass, progenitor mass and *total* lifetimes of the white dwarfs. The results indicate that the two new systems are probably ancient thick disk objects with ages of at least 6-9 Gyr. We also conduct searches of red dwarf and white dwarf compendia from SDSS data and the Lépine Shara Proper Motion (LSPM) catalog for additional common proper motion white dwarf-red subdwarf systems. Only seven new candidate systems are found, which indicates the rarity of these systems.

Subject headings: white dwarfs – binaries – subdwarfs – ages

1. Introduction

Subdwarfs are Galactic fossils that provide answers to questions concerning the age of the Milky Way, its early composition, the rate of star formation at early epochs, and the Galaxy's overall construction by the cannibalism of nearby small galaxies. Subdwarfs of K

¹Visiting Astronomer, Cerro Tololo Inter-American Observatory. CTIO is operated by AURA, Inc. under contract to the National Science Foundation.

and M types are presumably the most numerous stellar components of the early Galaxy, yet they are the types least studied because of their low luminosities. Subdwarfs are notoriously far more rare than disk stars, and therefore harder to identify and study. For example, of the 243 stellar systems now known within 10 pc of the Sun, only two are confirmed subdwarf systems (with accurate parallax and spectra): μ Cas AB (GJ 53 AB, [Fe/H] = -0.71 , Karaali et al. 2003) and CF UMa (GJ 451, [m/H] = -1.44 , Carney et al. 1994)

Although they are difficult to find, a widely applied strategy used to identify subdwarfs, selecting stars with high proper motions, can yield a rich sample of subdwarf candidates that can be targeted for more detailed observations. Selection by proper motion is highly successful because old stars tend to have large heliocentric velocities after billions of years of “heating” from many passages through the Galactic disk. For example, Schmidt (1975), Gizis and Reid (1999), and Digby (2003) have used high proper motion criteria to select potential subdwarfs and to determine the subdwarf luminosity function. However, we have found that only 19 (33%) of Schmidt’s 57 subdwarf candidates are, in fact, spectroscopically confirmed subdwarfs (Jao 2004), illustrating the significant contamination of proper motion samples by disk stars. Two observations are required to scrub samples of potential low mass subdwarfs of interlopers: (1) trigonometric parallax observations to confirm that candidates lie 1-3 magnitudes below the main sequence, and (2) spectroscopic observations to confirm that candidates have low metallicity (strength of the CaH and TiO bands in particular for the cool subdwarfs). Some subdwarf candidates have been identified by one of these observations, but within 60 pc there are currently only 58 K and M type subdwarfs confirmed by both types of observations (Jao 2004).

White dwarfs (WDs) are the end products of the evolution of stars with masses of $1 M_{\odot}$ to $8 M_{\odot}$. If we consider any typical initial stellar mass function, it is instantly clear that this makes WDs the most common end state of stellar evolution. Because of their large numbers, ability to be modeled effectively, and age dispersion spanning our Galaxy’s entire history, WDs provide important, interpretable clues about Galactic timescales. This potential was recognized many years ago by Schmidt (1959) in a study of star formation rates. Many developments have occurred since then in both observational and theoretical studies of WDs. Observationally, with modern telescopes we have been able to detect fainter objects, giving us more detailed information on the cool, old WDs (Bergeron et al. 2001), including those in globular clusters that are used to determine cluster ages (Richer et al. 1997; Hansen et al. 2002). Recent observations also suggest that an ancient WD population could exist in the Galactic halo that may constitute an important part of the baryonic dark matter (Oppenheimer et al. 2001), although this is still rigorously debated (see, e.g. Reid et al. 2001, Reylé et al. 2001, Davies et al. 2002, Silvestri et al. 2002, Salim et al. 2004 and Bergeron et al. 2005). Theoretically, models (Bergeron et al. 2001, Fontaine et al. 2001)

continue to improve our understanding of WDs, in particular for the cool WDs that are members of the Galactic thick disk or halo.

During our southern parallax program CTIOPI (Cerro Tololo Inter-American Observatory Parallax Investigation), we have stumbled upon two unusual WDs in systems with red subdwarfs, LHS 193AB and LHS 300AB¹ (Jao et al. 2005). These two systems contain the first WDs ever found to have confirmed subdwarf companions, based on accurate parallax and spectroscopy, thereby giving us powerful insight into the nature of old WDs in low metallicity systems. Two other systems like these have been mentioned in the literature, GJ 781AB (Gizis 1998) and LHS 2139/2140 (Gizis & Reid 1997), but both are speculative, being based on broad spectral features plus mass functions in unresolved binaries and noisy spectra of one component, respectively. A third system, reported in Silvestri et al. (2002), has been spectroscopically confirmed but no parallax is available. Table 1 lists all of these systems as well as new candidate systems discussed in section 5. In this work we present a detailed analysis of the only two such resolved systems with parallaxes, including photometric and spectroscopic observations and estimates of the WDs’ physical parameters. Using models from the literature, we then use the physical parameters of the WDs to estimate their ages, and thereby provide a link between these old objects and their low metallicity red subdwarf counterparts. Finally, we discuss the results in the context of Galactic stellar populations.

2. Observations

2.1. Photometry Observations and Reduction

Initial $V_JR_{KC}I_{KC}$ (hereafter, subscripts not shown) photometry observations for LHS 193AB and LHS 300AB were reported in Jao et al. (2005). Data were taken at the CTIO 0.9m telescope, using a 1024×1024 Tek CCD with image scale $0''.401 \text{ pixel}^{-1}$ during CTIOPI. An additional VRI observation set was recently acquired for LHS 300AB, and improved deconvolution techniques allow us to improve the photometry values for components in both systems. The aperture sizes applied to LHS 193B (aperture $4''$, separation $12''.6$) and LHS 300B (aperture $2''$, separation $4''.3$) in Jao et al. (2005) were large enough to include contaminating flux from the primary stars’ wings. A $1''$ aperture size is now used for the WD components in both systems, and the results are given Table 2. These improved results indicate that the two white dwarfs are not quite as red as reported in Jao et al. (2005),

¹Both systems have L447–10 and L395–13 identifiers, respectively, in the New Luyten Two-Tenth (NLTT) catalogue. However, in order to keep consistent with the IDs we used in Jao et al. (2003, 2005), the LHS IDs will be used throughout this manuscript.

although they are still among the reddest WDs known, as can be seen in Figure 1. In order to test the reliability of the small aperture photometry, we compared the results with those obtained by performing PSF fitting and removal of the bright primary component of each system and then recalculating the photometry. Results from both methods were entirely consistent within the observational errors. The final signal-to-noise errors in VRI for the red dwarf components are 0.001 mag, whereas for the WDs the errors are 0.04 mag and the total errors are (including Signal to noise, systematics and night-to-night variabilty) 0.03 for the SDs and 0.05 for the WDs.

Infrared photometry of the LHS 193 and LHS 300 systems in the JH bands (standard CIT/CTIO filters) have been obtained using the ANDICAM detector at the CTIO 1.3m telescope via SMARTS time. The IR Array for ANDICAM is a Rockwell 1024×1024 HgCdTe Hawaii Array with 18-micron pixels, providing an image scale of $0''.137 \text{ pixel}^{-1}$ and a field of view of $2''.4 \times 2''.4$. Observations made before February 2005 have a missing quadrant in the upper right corner due to a chip malfunction that has since been fixed.

The observations were carried out with the intent of doing differential photometry using reference stars with well determined 2MASS magnitudes. To optimize image quality we used a dithering pattern with offsets of $15''$. Because of the limited field of view, there were only 1 and 3 suitable reference stars for LHS 193B and LHS 300B, respectively, but all four reference stars have 2MASS JHK_s magnitude errors of less than 0.04. These reference stars were also checked for photometric stability by using already existing frames from the long term CTIOPI parallax project – they showed no signs of variability larger than 0.02 mag in the optical (and presumably even less in the infrared). The 2MASS photometry has been converted to the CIT system by using the second generation relations from Carpenter (2003)².

The images were corrected for bias and flat-fielded using standard IRAF procedures. The reduced science frames were used to obtain aperture photometry in Interactive Data Language (IDL). The reason for adopting IDL in this step was the necessity to remove precisely the contribution of the primary components in the LHS 193 and LHS 300 systems by fitting the non-uniform background and subtracting it. Even in the case LHS 193, where the separation is $12''.6$, the contribution of the primary component's wings is substantial at the location of the secondary, especially given the great magnitude difference of these two components (~ 7 magnitudes at J). After subtraction, the aperture photometry of the faint

²The first generation transformations are from Carpenter (2001), based on the 2MASS second incremental data. After the 2MASS all sky database was released, the transformations have been recalibrated and released on Carpenter's website at <http://www.astro.caltech.edu/~jmc/2mass/v3/transformations>.

secondary components and reference stars was completed using a series of apertures with radii of 3 to 9 pixels in steps of 0.5 pixels. The final adopted magnitude was the average of all these values with the uncertainty given by the standard deviation of the mean (0.08 mag for J and 0.1 mag for H).

2.2. Spectroscopy Observations and Reduction

Spectroscopic observations of LHS 193AB and LHS 300AB were made with the 1.5-m and 4-m telescopes at CTIO, respectively. For the observations on the 1.5-m, the R-C spectrograph with a Loral 1200×800 CCD camera was used with the #32 grating (in first order) at tilt 15.1° . The order-blocking filter OG570 was used, resulting in spectra covering 6000\AA to 9500\AA with a resolution of 8.6\AA . At the 4.0-m, the R-C spectrograph with a Loral $3K \times 1K$ CCD was used with the #181 grating (in first order) at tilt 58.8° . The order-blocking filter OG515 was used, resulting in spectra covering 5500\AA to 10000\AA with a resolution of 6\AA . The fringing effect on the 4-m spectra at wavelengths longer than $\sim 7000\text{\AA}$ has been removed by customized IDL routines. Reductions were carried out in the standard way using IRAF reduction packages. Wavelength and flux calibrations were done using *twodspec.apextract* within IRAF. Results are shown in Figure 2.

Because of the wide separation of the LHS 193AB system, the spectra were observed separately for each component. However, the spectrum labelled LHS 300A in Figure 2 is actually a combined spectrum. The contamination is negligible given the large magnitude difference between the two components ($\Delta V = 4.6$, $\Delta R = 4.9$, $\Delta I = 5.0$). A spectrum of LHS 300B only was obtained by carefully aligning the slit, although some contamination from the primary is still present.

3. Spectra of the Red Subdwarfs and White Dwarfs

A sample of cool subdwarfs was previously studied by Gizis (1997), who showed that the subdwarf absorption bands of CaH_n ($n=1-3$) and TiO are the best features to separate subdwarfs from main sequence stars between 6000\AA and 9000\AA (our spectral coverage). Here we apply the same spectroscopic index method for both primary stars, LHS 193A and LHS 300A. Results are presented in Figure 3. The spectroscopic indices show that both stars fall in the early M type subdwarf region. When combined with the HR diagram results shown in Figure 1, the two pieces of evidence confirm, unequivocally, that LHS 193A and LHS 300A are subdwarfs.

Spectra for each of the white dwarf secondaries are presented in Figure 2. Both spectra are noisy because these objects are faint, but LHS 193B shows no apparent features except for the telluric lines seen in all the spectra in Figure 2. LHS 300B does show some continuum structure, especially in the red region of the spectrum due to contamination from the bright primary. One prominent feature seen close to λ 8542 does not have the same width as the corresponding one in the primary component and no trace of the other two lines of the CaII triplet, to which it should belong, are present, indicating that it is probably due to residual cosmic rays. These objects would be traditionally classified as featureless DC white dwarfs. Ideally, higher S/N spectra are desirable to deconvolve any trace hydrogen absorption from the noise should it exist (H α is within this spectral coverage at 6563 Å). We tentatively conclude that neither WD spectrum has hydrogen absorption features, which justifies the use of helium-rich models to characterize these objects, as discussed in the next section.

4. Ages of the White Dwarf Components

One of the most interesting aspects of WDs in general is that they provide us with a means of determining the age of the system to which they belong. This is possible because the physics of WD cooling is relatively well-understood and unhindered by assumptions about nuclear reaction rates, among others, allowing for reliable models to be constructed. Many models have been published in the literature for the cooling of WDs over the past several years (see for example Wood 1990, Wood 1995, Benvenuto & Althaus 1998, Hansen 1999 and Montgomery et al. 1999 among others). Our goal in this section is to estimate the *total* ages of the LHS 193 and LHS 300 systems by summing each WD's cooling age and its main sequence lifetime. The set of models described in Bergeron et al. (1995) is used here to determine the cooling ages, as well as other stellar parameters. The choice of this model in particular is due to the fact that the author provides complete grids for various photometric filters and physical quantities of the WDs, making it possible to use interpolation procedures to get physical parameters from observed photometrical values. With these results, we utilize the initial to final mass relations of Wood (1992) and Iben & Laughlin (1989) to estimate the progenitor masses and consequent main sequence lifetimes. A modern revision of such relations is presented by Weidemann (2000) where they suggest a new form for this function. However, this revised relation is not significantly different from the one of Iben & Laughlin (1989), which we adopt here for consistency with the discussion of Wood (1992).

4.1. White Dwarf Physical Parameters and Cooling Ages

The models of Bergeron et al. (1995) provide us with bolometric corrections and color indices on various photometric systems calculated for an extensive grid of hydrogen- (DA) and helium-rich (non-DA) white dwarf model atmospheres. Absolute visual magnitudes, masses, and ages are obtained for each model from detailed evolutionary cooling sequences. For each set of filters, grids are calculated for DA and non-DA atmosphere models. The DA model grid covers a range from $T_{eff} = 1500K$ to $100000K$ and from $\log(g) = 7.0$ to 9.0 , while the non-DA model grid covers a range from $T_{eff} = 3500K$ to $30000K$ and from $\log(g) = 7.0$ to 9.0 . The grids are available for public use at: <http://www.astro.umontreal.ca/~bergeron/CoolingModels/>.

One important step in this procedure is to decide which set of models to use for the interpolation required to match observed parameters for each WD. Photometry alone is not enough to decide between DA or non-DA model atmospheres and spectroscopy should always be available to pinpoint the type of WD being studied. This is very important, especially for age determinations, because cooling times are strongly dependent on the type of model considered, i.e. non-DA models give different cooling ages for a given position in the $(V - I) \times M_V$ plane than the DA models. In the case of LHS 193B and LHS 300B, both spectra show no evidence of hydrogen lines (as discussed in section 3), indicating very low abundance of the element in the atmosphere. Thus, they were both studied with He model atmospheres.

We estimate the physical characteristics and ages of the WD components using the *VRIJH* photometry for LHS 193B and LHS 300B. To map the WDs into the model grids, we interpolated values in the $(V - R, M_V)$, $(V - I, M_V)$, $(V - J, M_V)$, $(V - H, M_V)$ planes for each object to find their surface gravities, effective temperatures, masses, and cooling ages. The independent determinations from these color combinations are then averaged to obtain a final value for each parameter. The routines take the regularly-gridded set of models and use a smooth quintic surface for the interpolation. The result is a two-dimensional floating-point array containing the interpolated surface, sampled at the grid points. The color and absolute magnitude combinations discussed above are then interpolated on this surface using cubic convolution interpolation. For more detail on the interpolation routines see IDL manual and documentation. Results are given in Table 3.

The reason for utilizing the values for $(V - R)$, $(V - I)$, $(V - J)$, $(V - H)$ and M_V is simply due to the nature of the model grids available and their properties. Other relations can be constructed but are of limited use because of overlapping curves for different surface gravity values, thereby introducing degeneracies. As an example, one could use the $(V - I, B - V)$ relation if these photometric values are available. However, if we plot the model grid for these parameters, we see that the curves for different surface gravity values overlap for

some sections of the diagram (as shown in Figure 4). Consequently, this particular color-color diagram is degenerate and would not provide meaningful results.

To determine the reliability of our method we compared our results with those of a “control” WD, GJ 283A with type DQ, which is the primary star of a binary system with an M6.0V main sequence red dwarf companion. This provides two opportunities for comparison — the WD has also been evaluated by Bergeron et al. (2001) so we can check the consistency of results, and the main sequence red dwarf is likely much younger than the red subdwarfs, LHS 193A and LHS 300A, so we should determine a younger cooling age for GJ 283A. Using our method and the observed values from Bergeron et al. (2001) for GJ 283A, we find differences of 1% in surface gravity, 4% in temperature, 14% in mass and 10% in cooling age. These differences are likely due to the nature of the interpolation process and on model grid resolution; we conclude that our procedure is sound. Derived cooling ages and other physical parameters for all three white dwarfs are listed in Table 3. We confirm that the GJ 283 system is significantly younger than the LHS 193 and LHS 300 systems.

4.2. White Dwarf Progenitor Masses and Main Sequence Lifetimes

Using relations presented in Wood (1992), we can estimate the progenitor masses of the WDs and their main sequence lifetimes via the following equations:

$$M_{WD} = A \times e^{(B \times (M/M_{\odot}))} \quad (1)$$

$$t_{MS} = 10 \times (M/M_{\odot})^{-2.5} Gyr \quad (2)$$

where M_{WD} is the mass of the white dwarf, A and B are constants (see description below), M is the mass of the progenitor (both masses in solar units), and t_{MS} is the main sequence lifetime in *Gyr*.

The constants in Equation 1 need to be defined so that a value of M can be determined. In this work we adopted three different prescriptions for these constants, two from Wood (1992) and one is from Iben & Laughlin (1989). The two prescriptions from Wood (1992) are the ones referred to in that work as Model D ($A = 0.40$ and $B = 0.125$) and Model E ($A = 0.35$ and $B = 0.140$). Model D in particular is what the author defines as the “Best Guess Model”. The third prescription uses the Initial–Final mass relation defined by Iben & Laughlin (1989). In this work we refer to these different prescriptions as Wood D, Wood E and Iben 89, respectively. The choice of these particular models is based on the

theoretical mass functions obtained from them. As mentioned in Wood (1992), the best fit to the observed mass function is achieved using Wood D. Wood E and Iben 89 are included as independent checks on the progenitor masses and main sequence lifetimes. Results for all three methods are given in Table 3.

4.3. White Dwarf Total Ages

The total ages of LHS 193B and LHS 300B are simply the sums of their main sequence lifetimes and their cooling ages, i.e. t_{cool} and t_{MS} given in Table 3. Given the various uncertainties in the methods used to determine both portions of the WDs’ *total* ages, we conclude that both systems have ages of 6-9 Gyr. By proxy, we conclude that the low metallicity subdwarf components have the same ages as their WD partners, thereby providing a link between WD ages and red dwarf metallicities.

5. The Rarity of Cool Subdwarf-White Dwarf Binaries

Given the utility of these WD-subdwarf pairs in investigating the link between age and metallicity, we have carried out searches for these systems in Sloan Digital Sky Survey (SDSS), the Lépine Shara Proper Motion (LSPM, see Lépine & Shara (2005) for details) northern hemisphere catalog and the wide common proper motion pairs reported by Chanamé & Gould (2004). In the SDSS data, West et al. (2004) have detected 60 subdwarfs from the analysis of nearly 8000 late type dwarfs. We compare the positions of these spectroscopically confirmed subdwarfs with the SDSS WD catalog of Kleinman et al. (2004) to reveal WD-subdwarf pairs. The WD catalog has coordinates (equinox 2000.0, epoch approximately 2000.0) and many proper motions for the objects, but the subdwarf catalog only has coordinates (equinox 2000.0). In order to find potential close binaries in the two catalogs, a coordinate comparison was carried out using a generous 5' search radius around each entry of the WD catalog. No subdwarfs were found in West et al. (2004) that were within 5' of any SDSS WD catalog entries.

Lépine & Shara (2005) have released the most comprehensive catalog of high proper motion stars in the northern sky, which contains nearly 62,000 stars with proper motions greater than $0.^{\circ}15 \text{ yr}^{-1}$. Populations of main sequence stars, subdwarfs, and white dwarfs found in the catalog can be separated effectively (although not perfectly) using proper motions and magnitudes to calculate each object’s reduced proper motion, H , as introduced by Luyten (1939) and defined as follows,

$$H = m + 5 \log \mu + 5, \quad (3)$$

where μ is the proper motion in seconds of arc per year and m is the apparent magnitude, V . The simple assumption is that proper motion is correlated with parallax, so that samples without parallax measurements can be investigated. Gizis & Reid (1999), Digby et al. (2003) and Salim & Gould (2003) have previously used this technique to separate subdwarfs from main sequence stars. Our search of the LSPM catalog utilizes the reduced proper motion diagram in Figure 5, which plots H_V vs. $V - J$ color. Because many faint objects in the LSPM catalog lack V band photometry, Lépine & Shara (2005) estimated the optical V band magnitudes from photographic plate B_J and R_F magnitudes. The vast majority of LSPM have reliable near infrared photometry from 2MASS. For those that do not, Lépine & Shara (2005) estimate J from plate I_N magnitudes.

We have defined rough boundaries, plotted in Figure 5, to indicate the WD region. All possible WD candidates within this region are compared with all other stars in the LSPM catalog to reveal companions, with the particular goal of finding subdwarf companions. The LSPM catalog has a coordinate accuracy of about ~ 90 mas and proper motion accuracy of ~ 10 mas yr^{-1} .

Two common proper motion binary searches were done, using the following criteria:

1. Separation of WD and candidate companion less than $1'$, proper motion difference less than $0''.1 \text{ yr}^{-1}$, and position angle of the proper motion difference less than 5 degrees;
2. Separation of WD and candidate companion between $1'$ and $5'$, proper motion difference less than $0''.01 \text{ yr}^{-1}$, and position angle of the proper motion difference less than 1 degree.

The results from the first search method are plotted in Figure 5. Companions of the WD candidates are shown as filled circles. There are 171 total binary system candidates, 8 of which are not shown on this figure because they lack $V - J$ colors. Of the 163 systems with colors, 108 companions are in the main sequence region, 48 companions are in the WD region (probable double degenerate binaries), and only seven stars are in the subdwarf region. These seven systems are the WD-subdwarf systems of interest here, and are listed in Table 1. Of these seven, four have estimated V and/or J magnitudes and are on the edges of the subdwarf region, whereas three have good photometry from 2MASS. We will carry out spectroscopic follow up observations to determine their luminosity classes. The second search revealed 24 candidate common proper motion binaries. Twenty of the companions

are in the main sequence region, four are in the WD region, and none are in the subdwarf region.

The third database from Chanamé & Gould (2004) Table 1 has been searched for the sdM-WD binaries. Although there are 1147 pairs of wide common proper motion binaries, only 58 systems been classified as “at least one component is a white dwarf” by them based on the reduced proper motion diagram. One system 880-460/880-461 (NLTT catalogue identifiers) is shown to be sdM-WD binary on the reduced proper motion diagram. However, after carefully checking the photographic plates having about 14 years time span, both stars do not appear to move at $0''.25 \text{ yr}^{-1}$ and both “components” do not have common proper motions as reported in the NLTT catalogue. Therefore, this system is not convincing and no sdM-WD has been found from Table 1 in Chanamé & Gould (2004).

We conclude that WD-subdwarf pairs are quite rare. The three searches revealed only seven candidate systems, and only three of those have reliable photometry. Accurate V and J photometry for more of the stars in LSPM might reveal additional candidate systems.

6. Discussion

The rarity of subdwarfs in the solar neighborhood increases our difficulty in understanding their physical parameters, including their sizes, masses, and even ages. The discovery of the two rare WD-subdwarf systems reported here provides a crucial step towards a better understanding of the star formation history of our Galaxy because these systems allow us to link the ages of the WDs to the metallicities of the subdwarfs. Figure 3 indicates that the metallicities of both LHS 193A and LHS 300A are $[m/H] \sim -0.5$ (details of the methodology are the subject of a future paper). Unfortunately, these systems are rare, so it will take considerable effort to build up a statistical database. Nevertheless, a careful reconnaissance may reveal enough systems to produce a map of age vs. metallicity that will provide valuable insight into the Galaxy’s past.

The HR diagram and spectroscopic analysis both indicate that the red components in the WD-subdwarf systems are true subdwarfs. From our astrometry results of the subdwarf components (Jao et al. 2005), we also know that the tangential velocities are indicative of an old population — 147 km/sec for LHS 193A and 183 km/sec for LHS 300AB. Comparison of our results to the kinematic study of low mass stars of Leggett (1992) (shown in the inset of Figure 1), both primaries appear to have halo-like kinematics. The WD *total* ages of 6-9 Gyr derived here indicate that the systems are not members of the young disk or extremely old halo, but they are probably members of the old disk (or young halo) population.

To estimate the *total* ages discussed above we calculated values of progenitor mass and main sequence lifetimes for two prescriptions of Wood (1992) as well as the relation proposed by Iben & Laughlin (1989). When comparing the progenitor masses determined for each star we see that there is a considerable difference when adopting one or another prescription for the initial to final mass relation. However, the final ages obtained are within the approximate error of 1 Gyr suggested by Wood (1992). This is a clear indication that although these prescriptions should be used with caution, reliable total age estimates are possible because the cooling time is the dominant factor. Figure 6 shows the three systems studied here in the $M/M_{\odot} \times T_{\text{eff}}$ diagram, with a background of cooling curve isochrones (solid lines) and corresponding *total* age curves (dotted lines) for the “Best Guess Model” of Wood (1992). Notice that LHS 300B is located at the convergence region of the *total* age curves and therefore it could be even older than the 6–9 Gyr estimate, given the uncertainty in its mass.

Uncertainties in WD cooling times and temperatures may cause the ages reported here to be in error. Fontaine et al. (2001) discuss in detail many current issues in WD cooling time calculations. Of particular interest to our work is the variation of cooling curves due to different adopted abundances for WD cores. The authors point out that discrepancies as large as 3.6 Gyr can occur for a given luminosity of $10^{-6} L_{\odot}$ by adopting either a pure O core or a pure C core. However, the cooling ages determined in this work are in the range of 1–7 Gyr, where this discrepancy should still be within our method uncertainty of 1 Gyr (see Figure 7 in Fontaine et al. (2001)). As an example of the kind of changes that may occur in WD models, Dufour et al (2005) showed that the temperatures of DQ WDs may be significantly lower than previous values, when model atmospheres including metals and molecules are considered. This in turn has a direct implication on the masses determined for these objects. They find that the mean masses of the DQ WDs are reduced from 0.72 to $0.61 M/M_{\odot}$, in better agreement with the non-DA WD mean mass. This effect may also be important for non-DA WD stars in general, as in our case, indicating that the ages estimated here should be taken as an upper limit.

The only other WD-subdwarf system with an estimated *total* age for the WD is LP164–51/52, for which Silvestri et al. (2005) identify the system as a halo candidate with an age estimate of 9.6 Gyr (Silvestri, private communication). This age is based on an assumed WD mass of $0.61 M_{\odot}$, and an interpolation of the same model grids used here, although for the ($V - I$ vs Age) and/or ($B - V$ vs Age) diagrams. However, this procedure could lead to erroneous age estimates if the mass value is incorrect by even $0.1 M_{\odot}$, as can be seen, for example, in our Figure 6 for a given temperature. Ideally, a trigonometric parallax will be determined for LP164–51/52 and the characterization of the system can be completed.

7. Conclusions

In this work we present accurate *VRIJH* and spectroscopy from 6000Å to 9000Å for two new WD-subdwarf systems, LHS 193AB and LHS 300AB. Astrometry and photometry clearly identify each system to be comprised of a WD and a red subdwarf. The featureless spectra indicate that both WDs are type DC. In combination with our astrometry, photometry, and spectroscopy, we use literature model grids for helium-rich atmospheres to determine the surface gravities, temperatures, masses, and cooling ages of the WDs.

With the cooling ages and masses of the WDs, we estimate progenitor masses and main sequence lifetimes for the objects, and add the cooling ages to derive *total* ages of 6-9 Gyr for both systems. To determine the progenitor masses, we use three different prescriptions to avoid biases toward any particular model, and confirm the approximate \sim 1 Gyr uncertainty in the ages suggested by Wood (1992). Although some work has been done on the subject of mapping the connection from progenitor mass to remnant mass (Weidemann 1987; Weidemann & Koester 1983) there is still not a reasonable final solution to this question and the values presented here may change with different models. We do not consider this to be a significant problem because the cooling age comprises most of the *total* age.

These are the first two WD-subdwarf system for which precise photometry, spectroscopy, and most importantly, parallaxes, are available. This unique combination allows us to link the ages of the WDs to the low metallicities of specific red subdwarfs for the first time. We find that these two systems are likely members of the thick disk population of the Galaxy, which is supported by the systems' large tangential velocities. Even when errors are considered, the systems are not likely to be members of the halo because the *total* ages are below the canonical age of 12 to 14 Gyr usually adopted for halo type objects (see Gilmore et al. (1989) and references therein for details). Accurate Radial velocity measurements, when combined with the accurate astrometry reported here, would also provide useful insights into the kinematic population of the two systems. Nonetheless, we find the compelling result that there exist ancient stars in the solar neighborhood of low metallicity that are fossils of the early star formation epochs of our Galaxy.

We appreciate the assistance of the members of the SMARTS Consortium, Rebeccah Winnick in particular, and staff at CTIO who made many of the observations reported here possible. The RECONS team at Georgia State University is supported by NASA's Space Interferometry Mission and GSU. This work has used data products from the Two Micron All Sky Survey, which is a joint project of the University of Massachusetts and the Infrared Processing and Analysis Center at California Institute of Technology funded by NASA and NSF.

REFERENCES

Benvenuto, O. G., & Althaus, L. G. 1998, MNRAS, 293, 177

Bergeron, P., Wesemael, F., & Beauchamp, A. 1995, PASP, 107, 1047

Bergeron, P., Leggett, S. K., & Ruiz, M. T. 2001, ApJS, 133, 413

Bergeron, P., Ruiz, M. T., Hamuy, M., Leggett, S. K., Currie, M. J., Lajoie, C.-P., & Dufour, P. 2005, ApJ, 625, 838

Bessel, M. S. 1990, A&AS, 83, 357

Carney, B. W., Latham, D. W., Laird, J. B., & Aguilar, L. A. 1994, AJ, 107, 2240

Carpenter, J. M. 2001, AJ, 121, 2851

Carpenter, J. M., 2003, <http://www.astro.caltech.edu/~jmc/2mass/v3/transformations/>

Chanamé, J., & Gould, A. 2004, ApJ, 601, 289

P. Dufour, P. Bergeron, G. Fontaine 2005, astro-ph/0503448 accepted for ApJ

Davies, M. B., King, A., & Ritter, H. 2002, MNRAS, 333, 463

Digby, A. P., Hambly, N. C., Cooke, J. A., Reid, I. N., & Cannon, R. D. 2003, MNRAS, 344, 583

Fontaine, G., Brassard, P., & Bergeron, P. 2001, PASP, 113, 409

Gilmore, G., Wyse, R. F. G., & Kuijken, K. 1989, ARA&A, 27, 555

Gizis, J. E. 1997, AJ, 113, 806

Gizis, J. E., & Reid, I. N. 1997, PASP, 109, 849

Gizis, J. E. 1998, AJ, 115, 2053

Gizis, J. E., & Reid, I. N. 1999, AJ, 117, 508

Hansen, B. M. S. 1999, ApJ, 520, 680

Hansen, B. M. S., et al. 2002, ApJ, 574, L155

Hawley, S. L., Gizis, J. E., & Reid, I. N. 1996, AJ, 112, 2799

Iben, I. J., & Laughlin, G. 1989, ApJ, 341, 312

Jao, W.-C., Henry, T. J., Subasavage, J. P., Bean, J. L., Costa, E., Ianna, P. A., & Méndez, R. A. 2003, AJ, 125, 332

Jao, Wei-Chun, Ph.D. thesis, Georgia State University

Jao, Wei-Chun, Henry, T. J., Subasavage, J. P., Brown, M. A., Ianna, P. A., Bartlett, J. L., Costa, E., & Méndez, R. A. 2005, AJ, 129, 1954

Karaali, S., Bilir, S., Karataş, Y., & Ak, S. G. 2003, Publications of the Astronomical Society of Australia, 20, 165

Kleinman, S. J., et al. 2004, ApJ, 607, 426

Leggett, S. K. 1992, ApJS, 82, 351

Lépine, S., & Shara, M. M. 2005, AJ, 129, 1483

Luyten, W. J., Bruce Proper Motion Survey III. The Stars of Large Proper Motion and the Luminosity Function, Minneapolis: University of Minnesota, 1939

Montgomery, M. H., Klumpe, E. W., Winget, D. E., & Wood, M. A. 1999, ApJ, 525, 482

Oppenheimer, B. R., Hambly, N. C., Digby, A. P., Hodgkin, S. T., & Saumon, D. 2001, Science, 292, 698

Reid, I. N., Sahu, K. C., & Hawley, S. L. 2001, ApJ, 559, 942

Reylé, C., Robin, A. C., & Crézé, M. 2001, A&A, 378, L53

Richer, H. B., et al. 1997, ApJ, 484, 741

Salim, S., & Gould, A. 2003, ApJ, 582, 1011

Salim, S., Rich, R. M., Hansen, B. M., Koopmans, L. V. E., Oppenheimer, B. R., & Blandford, R. D. 2004, ApJ, 601, 1075

Silvestri, N. M., Oswalt, T. D., & Hawley, S. L. 2002, AJ, 124, 1118

Silvestri, N. M., Hawley, S. L., & Oswalt, T. D. 2005, AJ, 129, 2428

Silvestri, N. M., Oswalt, T. D., & Hawley, S. L. 2002, AJ, 124, 1118

Schmidt, M. 1959, ApJ, 129, 243

van Altena, W. F., Lee, J. T., & Hoffleit, D. 1995, The General Catalogue of Trigonometric Stellar Parallaxes (4th ed.; New Haven: Yale Univ. Obs.)

Weidemann, V. 1987, A&A, 188, 74

Weidemann, V. 2000, A&A, 363, 647

Weidemann, V., & Koester, D. 1983, A&A, 121, 77

Weis, E. W. 1996, AJ, 112, 2300

West, A. A., et al. 2004, AJ, 128, 426

Wood, M. A. 1990, JRASC, 84, 150

Wood, M. A. 1992, ApJ, 386, 539

Wood, M. A. 1995, LNP Vol. 443: White Dwarfs, 443, 41

Table 1: WD-subdwarf binary candidates

Object	<i>VRI</i> Photometry	Spectroscopy	Parallax
LHS193AB	this work	this work	Jao et al. (2005)
LHS300AB	this work	this work	Jao et al. (2005)
LHS2139/2140 ^a	no	Gizis & Reid (1997)	no
GJ781AB ^b	Weis (1996)	Gizis (1998)	van Altena et al. (1995)
LP164-51/52	no	Silvestri et al. (2002)	no
LSPMJ0008+1634/1635	no	no	no
LSPMJ0846+4925E/W	no	no	no
LSPMJ0927+6210N/S	no	no	no
LSPMJ1200+4105N/S	no	no	no
LSPMJ1209+2448E/W	no	no	no
LSPMJ1539+5402N/S	no	no	no
LSPMJ1702+7158N/S	no	no	no
LSPMJ2100+3426E/W	no	no	no

^aHS 2140 has spectral features of an M-subdwarf, but LHS 2139 spectrum appears noisy but featureless.

^bGJ 781AB is a spectroscopic binary and has combined photometry reported in Weis (1996). GJ 781A, an M subdwarf, shows absorption lines broader than regular M dwarfs.

Table 2: $VRIJH$ photometry for binary systems.

object	<i>V</i>	<i>R</i>	<i>I</i>	# obs	<i>J</i>	<i>H</i>	# obs	π (mas)	Ref
LHS 193A	11.66	10.85	10.09	3	9.17	8.55	3	32.06 ± 1.65	Jao et al. 2005
LHS 193B	17.73	17.18	16.60	3	16.21	15.94	3	...	
LHS 300A	13.18	12.28	11.49	2	10.48	10.00	2	32.30 ± 1.85	Jao et al. 2005
LHS 300B	17.79	17.13	16.45	2	15.94	15.89	2	...	
GJ 283A	13.01	12.86	12.71	...	12.69	12.60	...	112.4 ± 2.7	van Altena et al. 1995
GJ 283B	16.54	14.68	12.43	...	10.14	9.61	

Note. — The *J* and *H* photometry have been converted from the 2MASS to CIT system, except for LHS 193B and LHS 300B, which were observed here and are already CIT. The optical photometry for GJ283 A and B is from Bessel (1990).

Table 3. Physical parameters and Ages for Studied Systems^a .

object	Log(g)	Teff	M_{WD}	t_{cool}	Wood D			Wood E			Iben 89		
					$M (M_{\odot})$	t_{MS}	t_{total}	$M (M_{\odot})$	t_{MS}	t_{total}	$M (M_{\odot})$	t_{MS}	t_{total}
LHS 193B	8.1	4934	0.60	6.5	3.3	0.5	7.0	3.9	0.3	6.8	2.0	1.7	8.2
LHS 300B	7.8	4705	0.48	5.0	1.4	4.2	9.1	2.2	1.4	6.3	<2.0	>1.8	6.7
GJ 283A	8.3	8457	0.77	1.6	5.3	0.2	1.7	5.8	0.1	1.7	4.1	0.3	1.9
GJ 283A ^b	8.2	8010	0.72	1.6	4.8	0.2	1.8	5.2	0.2	1.7	3.5	0.4	2.0
GJ 283A ^c	8.09	7710	0.63	1.45

^aAll ages and cooling times given in Gyr

^bthese are values obtained with our interpolation procedure using Bergeron (2001) observed values for GJ 283A.

^cValues obtained by Bergeron et al. (2001)

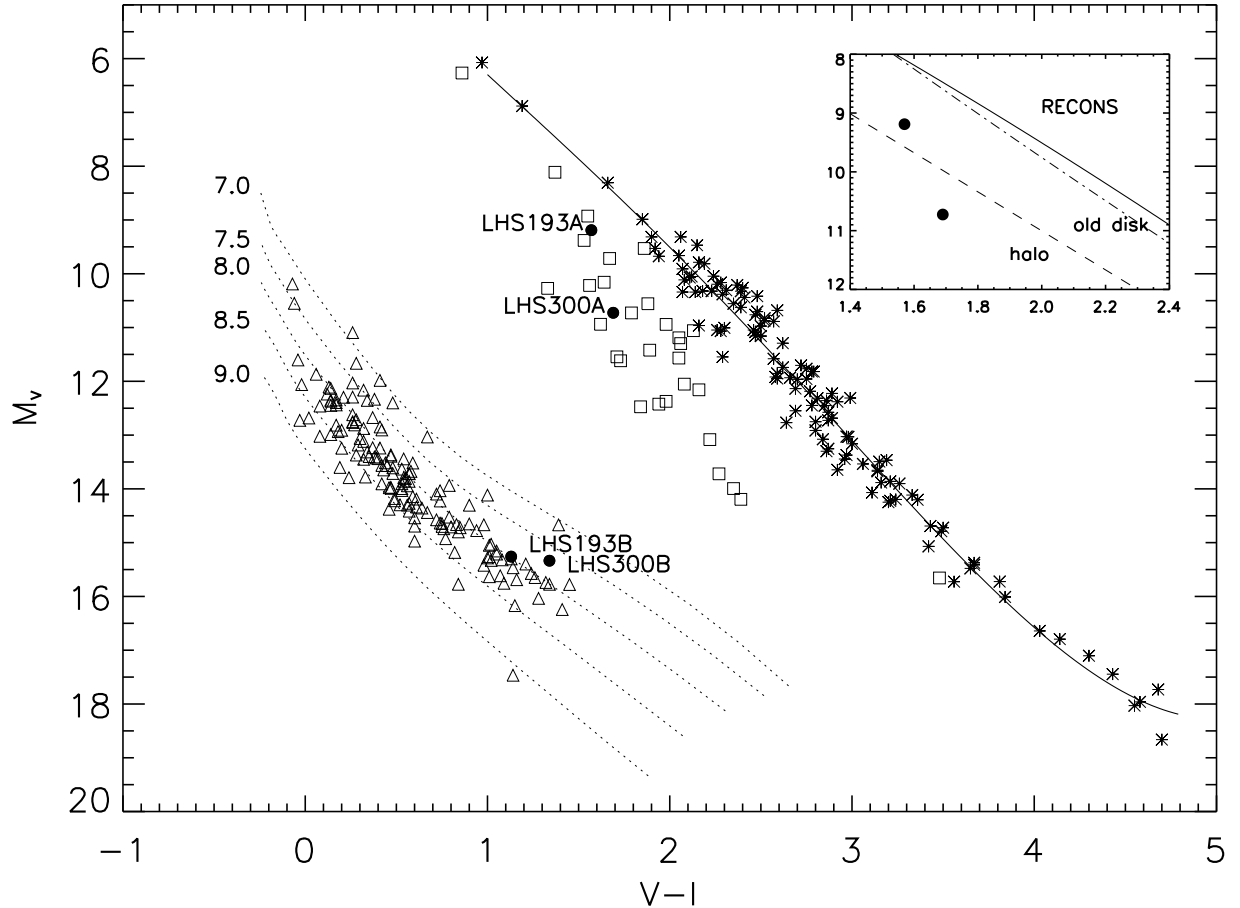


Fig. 1.— Components of the LHS 193 and LHS 300 systems are labeled with solid circles. The open squares represent subdwarfs with $\mu > 1.^{\circ}0 \text{ yr}^{-1}$ from Gizis (1997). Asterisks are RECONS stars (stars within 10pc) used to outline the main sequence, and the solid line indicates the best fitted line for these stars. Triangles are white dwarfs from Bergeron et al (2001). The dotted line shows different helium-rich cooling curves with $\log(g)$ labeled. The inset is a zoom-in for both primaries. The solid line is the same as defined above. The dash-dot and dash lines are best fits for old disk and halo stars, respectively, from Leggett (1992).

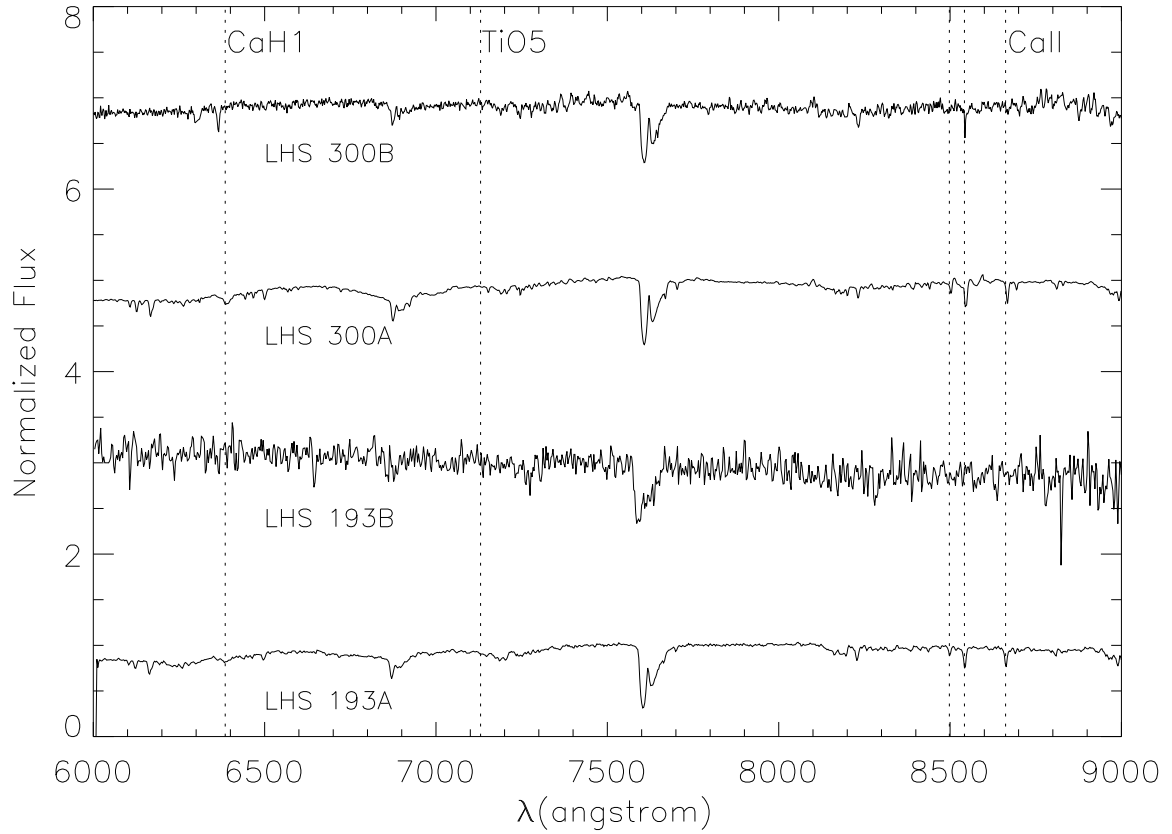


Fig. 2.— Spectra obtained for LHS 193AB and LHS 300AB normalized at 7500 Å (offset for clarity). These are combination of different spectra taken with different instruments, see text for details. The important absorption lines of CaII, as well as the center of the CaH1 and TiO5 bands are indicated with dotted lines.

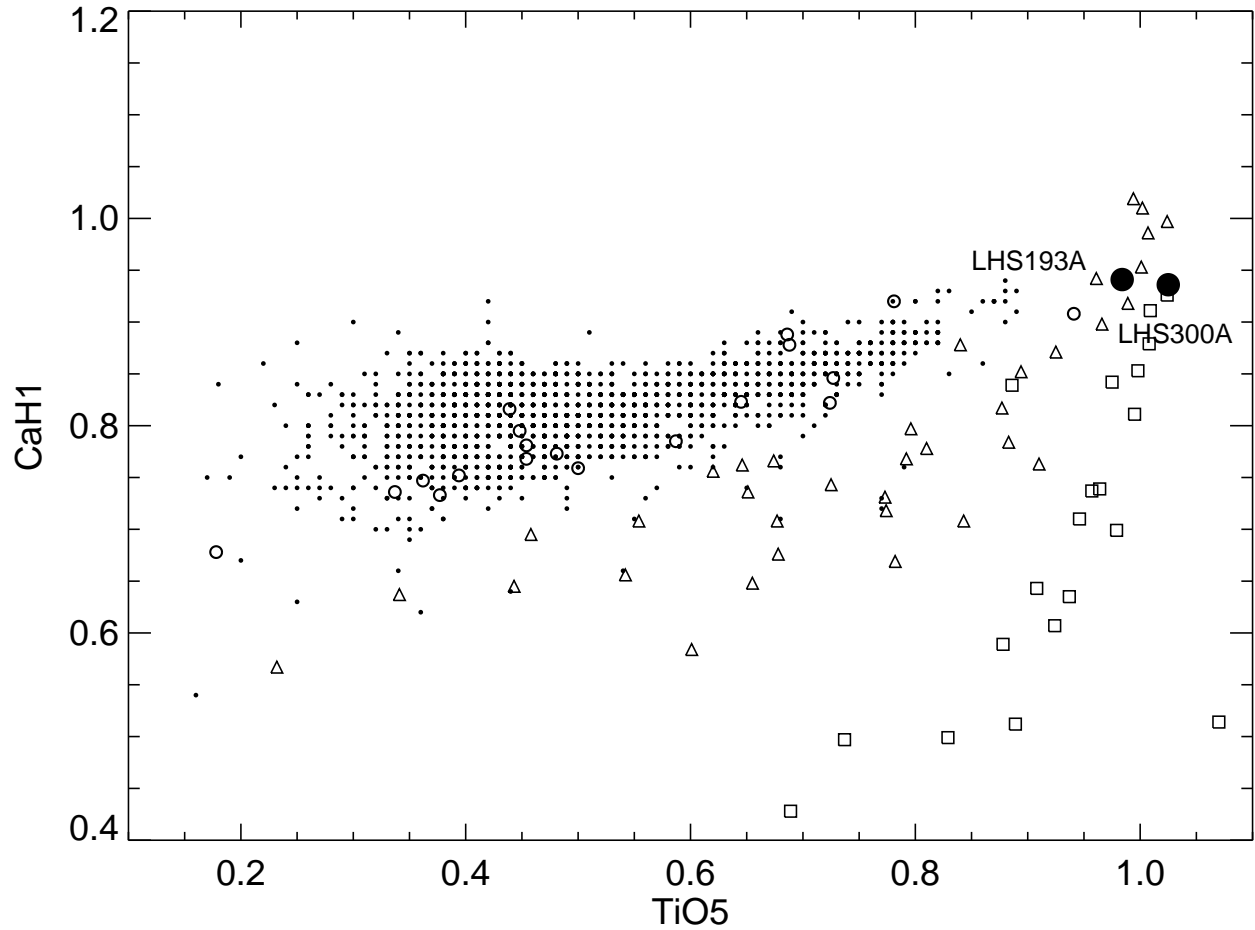


Fig. 3.— Stars classified as main sequence stars from Gizis (1997) appear as open circles, subdwarfs as open triangles and extreme-subdwarfs as open boxes. Small dots represent main sequence stars from Hawley et al. (1996) using the same indices. Two filled circles represent our two science stars, LHS 193A and LHS 300A. The CaH1 band is from 6380Å to 6390Å and the TiO5 band is from 7126Å to 7135Å.

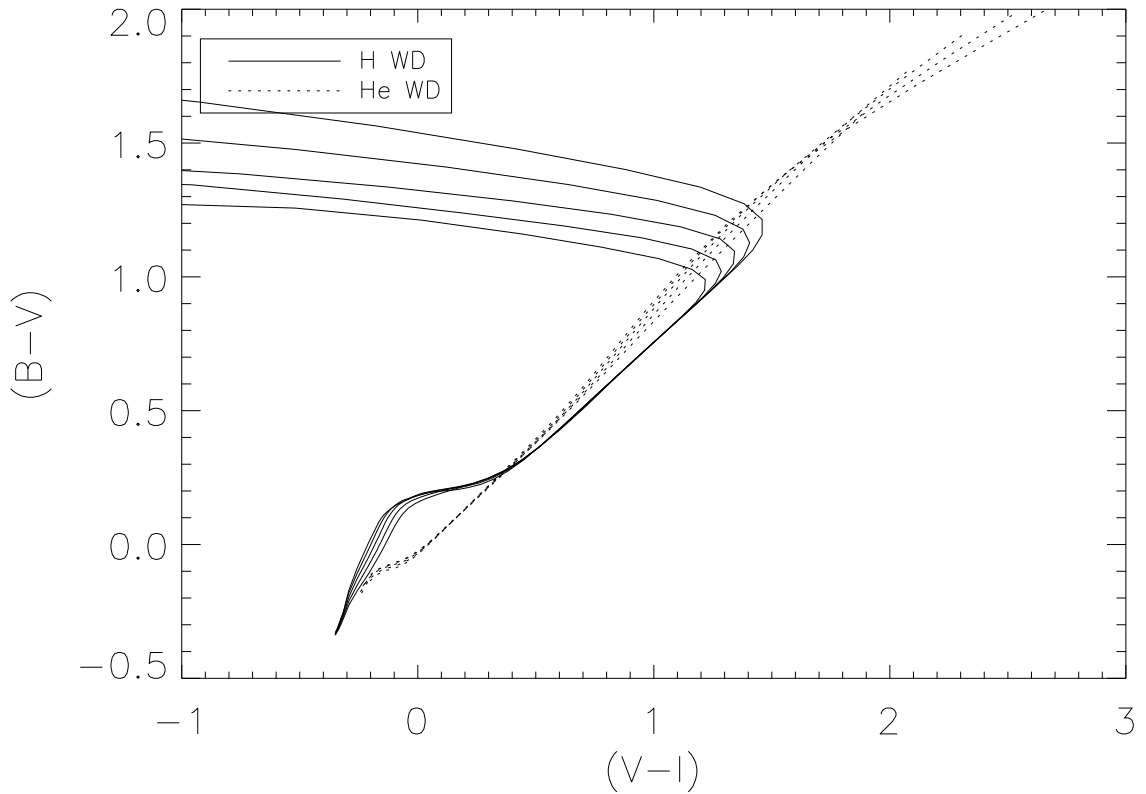


Fig. 4.— Model curves for DA (H models) and non-DA (He models) WDs for different $\log(g)$ values from 7.0 (top curve for DA models) to 9.0 (bottom curve for DA model) showing the degeneracy portions of this particular color-color relation (see text for details on the models used). The curves for the non-DA models cover the same $\log(g)$ range as the H models.

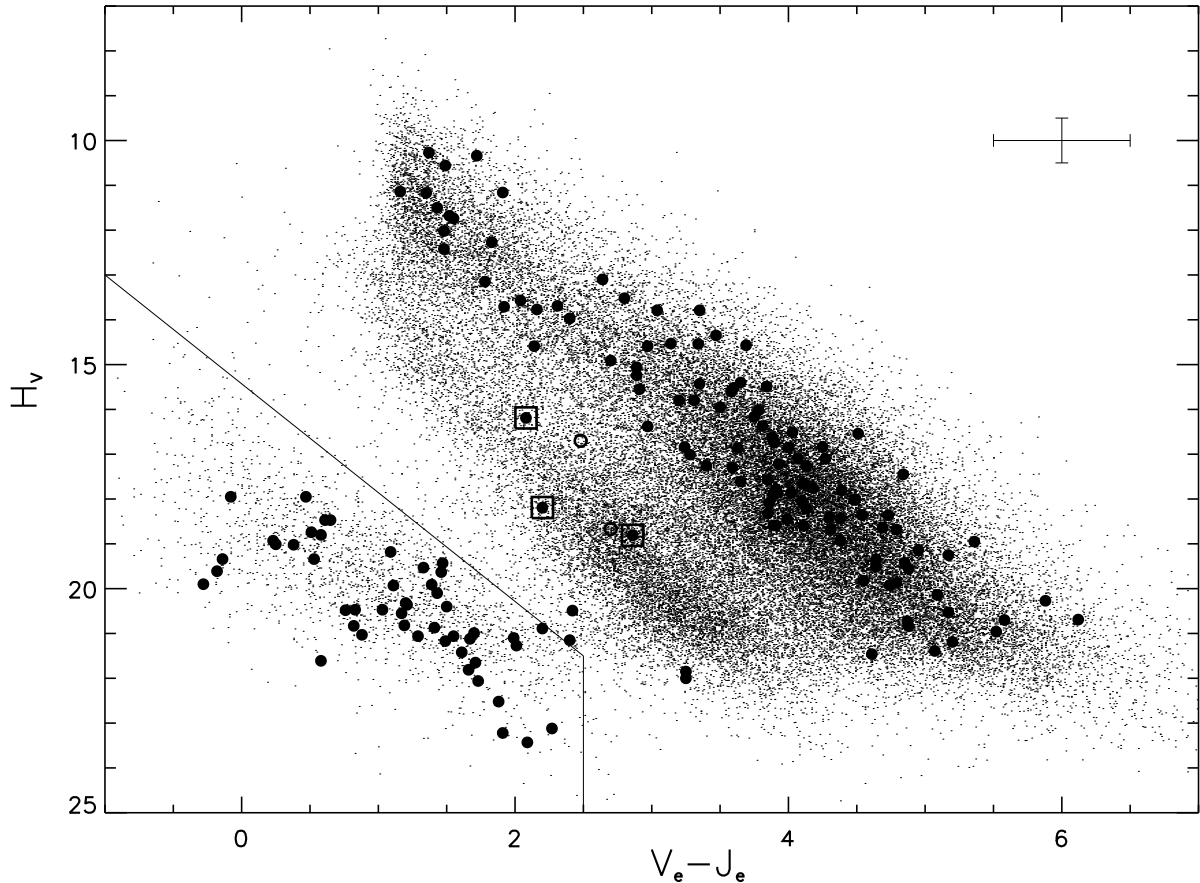


Fig. 5.— Reduced proper motion diagram for LSPM catalog. Three different luminosity populations can easily be seen. Stars to the lower left of the thin solid line are selected as “WD” candidates. Stars that are companions (less than 1' separation) to these “WD” are indicated as filled circles. Three boxed stars have observed J from 2MASS. The two open circles indicate LHS 193A (top) and LHS 300A (bottom) using V and J magnitudes reported here. The error bars are shown in the upper right side.

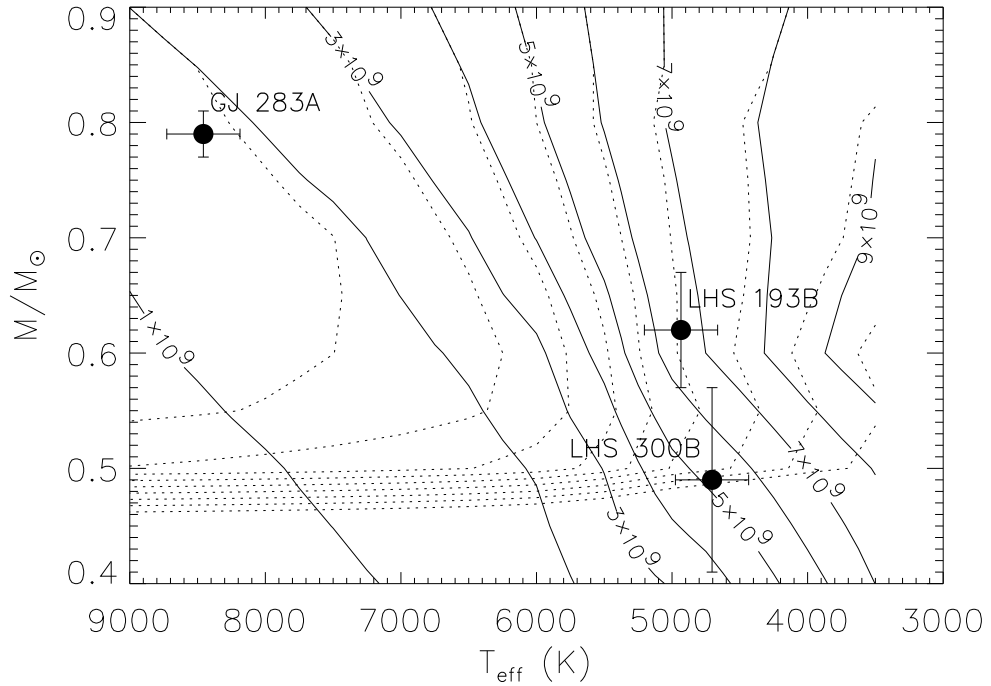


Fig. 6.— Position of the three systems studied in the $M/M_{\odot} \times T_{\text{eff}}$ diagram. Solid lines are the cooling age isochrones and dotted lines are *total* age isochrones (cooling age plus MS age) with units given in years. The dotted lines are drawn for the same isochrones values as the solid lines.